Valery V. Tuchin
Jürgen Popp
Valery Zakharov *Editors*

Multimodal Optical Diagnostics of Cancer

Springer

Multimodal Optical Diagnostics of Cancer

Valery V. Tuchin • Jürgen Popp
Valery Zakharov
Editors

Multimodal Optical Diagnostics of Cancer

Springer

Editors
Valery V. Tuchin
Department of Optics and Biophotonics
Saratov State University
Saratov, Russia

Valery Zakharov
Department of Laser and Biotechnical Systems
Samara National Research University
Samara, Russia

Jürgen Popp
Leibniz-Institute of Photonic Technology e.V. and Institute of Physical Chemistry and Abbe Center of Photonics
University of Jena
Jena, Thüringen, Germany

ISBN 978-3-030-44593-5 ISBN 978-3-030-44594-2 (eBook)
https://doi.org/10.1007/978-3-030-44594-2

This Springer imprint is published by the registered company Springer Nature Switzerland AG
The registered company address is: Gewerbestrasse 11, 6330 Cham, Switzerland

Preface

The purpose of this book is to outline the state-of-the-art optical approaches for the enhancement of medical diagnostics and earlier cancer detection and classification. The book brings together a description of the wide variety of optical techniques that have recently emerged for the specific study of the tumors of different organs and tissues. The appearance of this book was stimulated by the recent rapid progress in novel photonics technologies, the development of robust and cost-effective low-noise detectors and lasers, and fiber-optics devices. The multimodal approach provides a unique combination of structural, morphological, molecular, and metabolic information. The complexities of different methods of integration are compensated by the potential increase in both sensitivity and specificity of cancer diagnosis, screening, treatment monitoring, or image-guided intervention.

The diagnosis of cancer is a complex process and requires a number of diagnostic studies. But standard imaging modalities such as computed tomography, magnetic resonance imaging, and positron emission tomography require significant financial resources and infrastructure, which limits access to these modalities and excludes their usage for screening. In contrast, optical imaging strategies, with the potential for reduced cost and enhanced portability, are emerging as additional tools to facilitate the early detection and diagnosis of cancer. Many spectroscopic methodologies and optical imaging technologies have been established for nearly all kinds of cancer. However, the current gold-standard in cancer diagnosis is the examination of a neoplasm by the trained eye of a physician followed by histological examination of an invasive excisional biopsy of the tumor tissue specimen. Pathologists rely on the microscopic analysis of tissue samples or additionally employ immune histochemical or molecular pathological analyses for a more precise diagnosis, classification, and prognosis regarding the cancerous tumor. In the majority of cases, the pathologist works with fixated and embedded tissue samples or, at least, with frozen sections. Intrinsically, the histological process is time-consuming. It is obvious that new methods and approaches are required for quick and reliable *in vivo* production of diagnostically relevant additional information. The optical methods meet these challenges through the implementation of molecular sensitive spectroscopic methods, including linear and nonlinear Raman

spectroscopy and its combination with other spectroscopic/optical modalities to a multimodal imaging approach for precise surgical guidance and intraoperative histopathologic examination of tissue.

However, due to the rather long acquisition times of spectroscopic tissue examination, the scanning of larger regions is quite challenging. This problem can be circumvented by combining detailed tumor spectral study with a fast imaging technique providing a quick selection of the region of interest (ROI). At the same time, the diagnostic accuracy depends as on the sensitivity of cancer detection as on the precision of correct ROI selection. Therefore, each optical imaging method also needs to be optimized for cancer detection and a multimodal approach should provide a synchronous sequential multilevel refinement of the diagnosis, both by spatial localization and cancer type detection. Hyperspectral imaging (HIS), optical coherence tomography (OCT), or fluorescence lifetime imaging (FLIM) offers a great potential for such a combination with the possibility of fiber-optics implementation suitable for clinical conditions.

Expanding the role of spectral analysis and optical imaging became a reality in global cancer management, including screening, early detection at the point-of-care, biopsy guidance, and real-time histology. In combination with online data analysis and multivariate statistics, multimodal spectral diagnostics and optical imaging have the potential to aid in the high-sensitive detection and management of precancer and early cancer by combining the tissue topology features and chemical composition.

This book is divided into four parts: Part I *Tumor Tissue Optics and Multimodal Microscopy* (Chaps. 1–4); Part II *Diffuse Spectroscopy and Fluorescence Analysis for Cancer Detection* (Chaps. 5–7); Part III *Raman Spectroscopy and Cancer Diagnostics* (Chaps. 8–10); and Part IV *Multimodal Cancer Imaging* (Chaps. 11–16).

Part I describes the tissue optical properties and their alteration with cancer progression. The malignant tissue alteration results in specific changes in nucleic acid, protein, lipid, and carbohydrate quantities of neoplastic cells. It is the basis for any optical cancer diagnostic applications, which might distinguish the tissue strongly associated with cancer development. The morphologic and biochemical changes that occur with malignant tissue are numerous and in many cases depend on the specific type and location of the cancer.

Chapter 1 reviews the light scattering spectroscopic methods and different approaches for tumor tissue optical properties and spectral features characterization. The inverse Monte Carlo simulation and diffuse approximations are used for modeling of light scattering in tumor and normal tissues. The physiological and optical properties of various types of lung, breast, colorectal, prostate, cervical, bladder, stomach, liver, kidney, skin, oral, and brain cancer are considered. The biochemical diagnostic models have been discussed as an instrument that helps to derive the morphological and biochemical composition, the functional state of cellular metabolism, and, as a result, determine the key features for the pathologist diagnostic decisions for appropriate cancer treatment.

In Chap. 2, the authors discuss the enhancement of optical diagnostics of tumors by using optical clearing (OC) methods. The OC-assisted optical imaging techniques

allow for acquiring high-resolution structural and functional images of neoplasms and their microvasculature. The monitoring of OC agents diffusion in tissues with high temporal and depth resolution allows one to differentiate healthy from malignant tissues.

The application of fluorescence lifetime imaging (FLIM) for recognition of changes in structural information accompanied by certain biochemical processes in living organisms is explored in Chap. 3. This chapter describes three main techniques on the basis of fluorescence time-resolved measurements—microscopic, spectroscopic, and macroscopic—and provides multiple examples of their applications in probing metabolism in cancer.

Chapter 4 describes the imaging of extracellular vesicles, including exosomes, for diagnosis, monitoring, and prediction of cancer. Different methods of light scattering, fluorescence, and single- and two-photon resonance absorption for exosome morphology and size measurements are presented.

In Part II, Chap. 5, the authors review the application of functional near-infrared spectroscopy to cancer diagnostics and therapy monitoring. It is discussed the capabilities of tissue differentiation, imaging of microvasculature and blood oxygenation concentrations, the possibility of brain cancer detection, and enhancement of noninvasive diagnostics in combination with other imaging modalities.

Chapter 6 describes the methods of volatile organic compounds measurements and details the spectral analysis of breath air samples for understanding specific biochemical processes and as a diagnostic tool for lung cancer diagnosis. High accuracy of multiclass classification of patients with several pulmonary diseases was demonstrated using a set of binary support vector machine classifiers.

A combined light-induced autofluorescence analysis and diffuse reflectance spectroscopy for the diagnosis of skin tumors are investigated in Chap. 7. It was demonstrated the preference of autofluorescence methods for detection and discrimination of nonpigmented skin tumors, but the whole set of benign, dysplastic, and malignant cutaneous lesions can be diagnosed with high sensitivity and specificity only with a multimodal approach, which serves as an “optical biopsy” tool.

Part III presents Raman spectroscopy as an especially potent technology with respect to molecular sensitivity providing detection of subtle changes in morphology and the distribution of endogenous molecular markers connected to disease initiation and disease progression in a label-free and noninvasive manner. Chapter 8 discusses the application of Raman spectroscopy in combination with advanced multivariate statistical analysis as a universal and cost-effective method of early cancer diagnosis and presents the benefits and the risks of the methodology.

The authors of Chap. 9 discuss the methods of Raman signal enhancement effects such as surface-enhanced Raman scattering, coherent anti-Stokes Raman scattering, and stimulated Raman scattering. Applications of Raman-based approaches for cancer diagnostics are summarized. Complementary optical methods including autofluorescence, optical coherence tomography, second harmonic generation, and two-photon excited fluorescence in combination with Raman scattering as multicontrast modalities are presented for pathological screening of cancer cells and tissues under *ex vivo* and *in vivo* conditions.

Chapter 10 compares the discussed Raman spectroscopic methods for optical analysis and screening of malignant and benign skin tissues. The clinical applications of skin cancer screening using a multimodal approach and *in vivo* Raman spectroscopy are presented.

Part IV describes different aspects of multimodal cancer imaging. In Chap. 11, the optical instruments for minimally invasive interventions in abdominal surgery are considered. Fine-needle optical probes with immediate comparison of tumor and healthy tissue optical properties are presented for the determination of the tissue state, in particular, for the diagnosis of hepatocellular carcinoma. The integration of multimodal fiber-optical probes with standard semiautomatic biopsy systems is discussed.

Chapter 12 describes the applications of multimodal optical coherence tomography (OCT) for characterizing tumorous tissues, including polarization-sensitive OCT providing complementary images in the initial and cross-polarization channels (CP-OCT), label-free angiography (OCA), and compressional variant of OCT-based elastography (OCE). The principles of realization and examples of various biomedical applications are considered for each modality. The authors present the results of using CP-OCT for detection of tumorous and non-tumorous regions in brain and breast tissues, application of OCA for monitoring the results of photodynamic therapy of murine model tumor CT26 and patients' basal cell carcinoma, utilization of OCA for studying mucositis on patients during radiation therapy, as well as monitoring of tumor response to chemotherapy with OCE.

Different statistical, frequency, and stochastic methods of texture analysis of dermatoscopic and OCT images for differentiation of various malignant and benign tumors are discussed in Chap. 13. The recognition of various tumors contemporaneously with a high-score identification of a tumor type is demonstrated in real clinical conditions by calculating comparative personal textural descriptors and implementation of multi-texture analysis when used texture features (Haralick, Tamura, Gabor, Markov Random Field, Complex Directional Field, Fractal Dimensions) complement each other.

Chapter 14 is dedicated to the specification of hyperspectral imaging devices based on acousto-optical tunable filters and their application for the detection and recognition of skin cancer. The basic concepts related to this technology are detailed. The applicability of hyperspectral imagers for endoscopic, microscopic, and macroscopic studies, as well as image reconstruction is demonstrated for different HSI schemes. The details of skin hyperspectral image analysis are presented along with the accuracy of a skin neoplasm detection.

Chapter 15 focuses on innovations using inelastic Raman scattering analysis for molecular fingerprinting of tissue combined with morphological information obtained from OCT. The combination of Raman and OCT, particularly recording co-localized three-dimensional information, could lead to a new form of diagnostic or screening tool for cancer studies.

A description of Terahertz (THz) spectroscopy and imaging for label-free diagnosis of malignancies with different nosology and localization is presented in Chap. 16. The brief introduction to THz technology, peculiarities of THz-wave–tissue

interactions, and THz pulsed spectroscopy are provided. The authors discuss THz imaging of brain tumors *ex vivo* and *in vivo* for mice and rat glioma models, human brain gliomas of different grades, as well as the pilot measurement of human brain meningioma.

This book is aimed at researchers, postgraduate and undergraduate students, laser engineers, biomedical engineers, and physicians who are interested in designing and applying laser and optical methods and instruments for cancer diagnostics and treatment, general application of optical methods in medicine and the medical device industry. Because of the large amount of fundamental and basic research on optical methods presented in this book, it should be useful for a broad audience including students and physicians. Physicians and biomedical engineers will be particularly interested in the chapters covering clinical applications and instrumentation. Optical engineers will also find many critical applications to stimulate novel ideas of laser and optical design.

Finally, the editors would like to thank all the authors who devoted their precious time to contribute very interesting and knowledgeable chapters, all who helped us in the preparation of the book, authors and publishers for their permission of reproducing their figures in this book, and the editorial staff of the publisher.

Saratov, Russia — Valery V. Tuchin
Jena, Germany — Jürgen Popp
Samara, Russia — Valery Zakharov

Contents

Contributors

Dmitry N. Artemyev Department of Laser and Biotechnical Systems, Samara National Research University, Samara, Russian Federation

Alexey N. Bashkatov Department of Optics and Biophotonics, Saratov State University, Saratov, Russian Federation

Laboratory of Biophotonics, Tomsk State University, Tomsk, Russian Federation

Wolfgang Becker Becker & Hickl GmbH, Berlin, Germany

Sheyh-Islyam T. Beshplav Burdenko Neurosurgery Institute, Moscow, Russian Federation

Alexey V. Borisov Department of Physics with a Course of Higher Mathematics, Siberian State Medical University, Tomsk, Russian Federation

Department of General and Experimental Physics, National Research Tomsk State University, Tomsk, Russian Federation

Ekaterina G. Borisova Institute of Electronics, Bulgarian Academy of Sciences, Sofia, Bulgaria

Saratov State University, Saratov, Russian Federation

Ivan A. Bratchenko Department of Laser and Biotechnical Systems, Samara National Research University, Samara, Russian Federation

Lyudmila A. Bratchenko Department of Laser and Biotechnical Systems, Samara National Research University, Samara, Russian Federation

Alla B. Bucharskaya Saratov State Medical University, Saratov, Russian Federation

Mingzhou Chen SUPA, School of Physics and Astronomy, University of St Andrew, St Andrews, Great Britain

Kishan Dholakia SUPA, School of Physics and Astronomy, University of St Andrew, St Andrews, Great Britain

Irina N. Dolganova Bauman Moscow State Technical University, Moscow, Russian Federation

Institute of Solid State Physics of the Russian Academy of Sciences, Moscow, Russian Federation

Viktor Dremin Orel State University, Orel, Russian Federation

University of Oulu, Oulu, Finland

Andrey Dunaev Orel State University, Orel, Russian Federation

Vadim Elagin Privolzhsky Research Medical University, Nizhny Novgorod, Russian Federation

Grigory Gelikonov Institute of Applied Physics RAS, Nizhny Novgorod, Russian Federation

Valentin Gelikonov Institute of Applied Physics RAS, Nizhny Novgorod, Russian Federation

Elina A. Genina Department of Optics and Biophotonics, Saratov State University, Saratov, Russian Federation

Laboratory of Biophotonics, Tomsk State University, Tomsk, Russian Federation

Natalia Gladkova Privolzhsky Research Medical University, Nizhny Novgorod, Russian Federation

Ekaterina Gubarkova Privolzhsky Research Medical University, Nizhny Novgorod, Russian Federation

Valery E. Karasik Bauman Moscow State Technical University, Moscow, Russian Federation

Irina Kasatkina Institute of Applied Physics RAS, Nizhny Novgorod, Russian Federation

Alexander G. Khramov Department of Technical Cybernetics, Samara National Research University, Samara, Russian Federation

Image Processing Systems Institute of RAS - Branch of the FSRC “Crystallography and Photonics” RAS, Samara, Russian Federation

Yulia A. Khristoforova Department of Laser and Biotechnical Systems, Samara National Research University, Samara, Russian Federation

Elena Kiseleva Privolzhsky Research Medical University, Nizhny Novgorod, Russian Federation

Lobachevskiy State University of Nizhny Novgorod, Nizhny Novgorod, Russia Federation

Yury V. Kistenev Laboratory of Biophotonics, National Research Tomsk State University, Tomsk, Russian Federation

Department of Physics with a Course of Higher Mathematics, Siberian State Medical University, Tomsk, Russian Federation

Semyon G. Konovalov Department of Laser and Biotechnical Systems, Samara National Research University, Samara, Russian Federation

Vesa Korhonen Oulu University Hospital, Oulu, Finland

Sergey V. Kozlov Department of Oncology, Samara State Medical University, Samara, Russian Federation

Samara Regional Clinical Oncology Dispensary, Samara, Russian Federation

Christoph Krafft Leibniz Institute of Photonic Technologies, Jena, Germany

Sergey Ksenofontov Institute of Applied Physics RAS, Nizhny Novgorod, Russian Federation

Vladimir N. Kurlov Institute of Solid State Physics of the Russian Academy of Sciences, Moscow, Russian Federation

Sergey Kuznetsov Privolzhsky Research Medical University, Nizhny Novgorod, Russian Federation

Igor K. Lednev Department of Chemistry, University at Albany, State University of New York, Albany, NY, USA

Maria M. Lukina Privolzhsky Research Medical University (PRMU), Nizhny Novgorod, Russian Federation

Alexander S. Machikhin Scientific and Technological Center of Unique Instrumentation of the Russian Academy of Sciences, Moscow, Russian Federation

Andrian Mamoshin Orel State University, Orel, Russian Federation

Orel Regional Clinical Hospital, Orel, Russian Federation

Anna Maslennikova Privolzhsky Research Medical University, Nizhny Novgorod, Russian Federation

Lev Matveev Institute of Applied Physics RAS, Nizhny Novgorod, Russian Federation

Alexander Matveyev Institute of Applied Physics RAS, Nizhny Novgorod, Russian Federation

Alexander Moiseev Institute of Applied Physics RAS, Nizhny Novgorod, Russian Federation

Alexander A. Moryatov Department of Oncology, Samara State Medical University, Samara, Russian Federation

Samara Regional Clinical Oncology Dispensary, Samara, Russian Federation

Oleg O. Myakinin Department of Laser and Biotechnical Systems, Samara National Research University, Samara, Russian Federation

Teemu Myllylä University of Oulu, Oulu, Finland

Luís M. C. Oliveira School of Engineering, Physics Department, Polytechnic Institute of Porto, Porto, Portugal

Centre of Innovation in Engineering and Industrial Technology, ISEP, Porto, Portugal

Andrey E. Orlov Samara Regional Clinical Oncology Dispensary, Samara, Russian Federation

Anton Plekhanov Privolzhsky Research Medical University, Nizhny Novgorod, Russian Federation

Jürgen Popp Leibniz Institute of Photonic Technologies, Jena, Germany

Institute of Physical Chemistry and Abbe Center of Photonics, Jena, Germany

Elena Potapova Orel State University, Orel, Russian Federation

Alexander A. Potapov Burdenko Neurosurgery Institute, Moscow, Russian Federation

Vitold E. Pozhar Scientific and Technological Center of Unique Instrumentation of the Russian Academy of Sciences, Moscow, Russian Federation

Nicole M. Ralbovsky Department of Chemistry, University at Albany, State University of New York, Albany, NY, USA

Dmitry S. Raupov Department of Laser and Biotechnical Systems, Samara National Research University, Samara, Russian Federation

Igor V. Reshetov First Moscow State Medical University (Sechenov University), Moscow, Russian Federation

Elena Sedova Privolzhsky Research Medical University, Nizhny Novgorod, Russian Federation

Vladislav I. Shcheslavskiy Becker & Hickl GmbH, Berlin, Germany

Pavel Shilyagin Institute of Applied Physics RAS, Nizhny Novgorod, Russian Federation

Marina V. Shirmanova Privolzhsky Research Medical University (PRMU), Nizhny Novgorod, Russian Federation

Marina Sirotkina Privolzhsky Research Medical University, Nizhny Novgorod, Russian Federation

Alexander Sovetsky Institute of Applied Physics RAS, Nizhny Novgorod, Russian Federation

Dmitriy Terpelov Institute of Applied Physics RAS, Nizhny Novgorod, Russian Federation

Petranka Troyanova University Hospital "Tsaritsa Yoanna – ISUL", Sofia, Bulgaria

Valery V. Tuchin Department of Optics and Biophotonics, Saratov State University, Saratov, Russian Federation

Laboratory of Biophotonics, Tomsk State University, Tomsk, Russian Federation

Laboratory of Laser Diagnostics of Technical and Living Systems, Institute of Precision Mechanics and Control of the Russian Academy of Sciences, Saratov, Russian Federation

Laboratory of Molecular Imaging, Bach Institute of Biochemistry, Research Center of Biotechnology of the Russian Academy of Sciences, Moscow, Russian Federation

Laboratory of Femtomedicine, ITMO University, St. Petersburg, Russian Federation

Alex Vitkin University of Toronto and University Health Network, Toronto, ON, Canada

Dmitry Vorontsov Privolzhsky Research Medical University, Nizhny Novgorod, Russian Federation

Denis A. Vrazhnov Department of General and Experimental Physics, National Research Tomsk State University, Tomsk, Russian Federation

Laboratory of Molecular Imaging and Photoacoustics, Institute of Strength Physics and Materials Science of Siberian Branch Russian Academy of Sciences, Tomsk, Russian Federation

Konstantin Yashin Privolzhsky Research Medical University, Nizhny Novgorod, Russian Federation

Natalia V. Yunusova Tomsk National Research Medical Center of the Russian Academy of Sciences, Tomsk, Russian Federation

Department of Biochemistry and Molecular Biology with a Course of Clinical Laboratory Diagnostics, Siberian State Medical University, Tomsk, Russian Federation

Elena V. Zagaynova Privolzhsky Research Medical University (PRMU), Nizhny Novgorod, Russian Federation

Lobachevskiy State University of Nizhny Novgorod, Nizhny, Novgorod, Russian Federation

Vladimir Zaitsev Institute of Applied Physics RAS, Nizhny Novgorod, Russian Federation

Valery P. Zakharov Department of Laser and Biotechnical Systems, Samara National Research University, Samara, Russian Federation

Kirill I. Zaytsev Prokhorov General Physics Institute of the Russian Academy of Sciences, Moscow, Russian Federation

Bauman Moscow State Technical University, Moscow, Russian Federation

Evgeny Zherebtsov Orel State University, Orel, Russian Federation

University of Oulu, Oulu, Finland

Part I
Tumor Tissue Optics and Multimodal Microscopy

Chapter 1
Malignant Tissue Optical Properties

Alexey N. Bashkatov, Valery P. Zakharov, Alla B. Bucharskaya, Ekaterina G. Borisova, Yulia A. Khristoforova, Elina A. Genina, and Valery V. Tuchin

1.1 Introduction

Despite the development of medicine, cancer remains one of the most dangerous diseases nowadays. World Health Organization (WHO) has reported 18.1 million new cancer cases and 9.6 million cancer deaths in 2018 [1]. Therefore, the detection and treatment of cancer is one of the most challenges for medicine in the twenty-first century. An effective solution of the problem is the use of modern

A. N. Bashkatov (✉) E. A. Genina
Department of Optics and Biophotonics, Saratov State University, Saratov, Russian Federation

Laboratory of Biophotonics, Tomsk State University, Tomsk, Russian Federation
e-mail: bashkatovan@sgu.ru; geninaea@sgu.ru

V. P. Zakharov · Y. A. Khristoforova
Department of Laser and Biotechnical Systems, Samara National Research University, Samara, Russian Federation
e-mail: zakharov@ssau.ru

A. B. Bucharskaya
Saratov State Medical University, Saratov, Russian Federation
e-mail: Ckp@sgmu.ru

E. G. Borisova
Institute of Electronics, Bulgarian Academy of Sciences, Sofia, Bulgaria
e-mail: borisova@ie.bas.bg

V. V. Tuchin
Department of Optics and Biophotonics, Saratov State University, Saratov, Russian

Laboratory of Biophotonics, Tomsk State University, Tomsk, Russian

Laboratory of Laser Diagnostics of Technical and Living Systems, Institute of Precision Mechanics and Control of the Russian Academy of Sciences, Saratov, Russian

Laboratory of Molecular Imaging, Bach Institute of Biochemistry, Research Center of Biotechnology of the Russian Academy of Sciences, Moscow, Russian
e-mail: tuchinvv@mail.ru

V. V. Tuchin et al. (eds.), *Multimodal Optical Diagnostics of Cancer*,
https://doi.org/10.1007/978-3-030-44594-2_1

interdisciplinary technologies. Most often, if the tumor is diagnosed earlier and treated, the patient will have a better prognosis and much greater opportunities for complete recovery. Many recent technological innovations have used physics principles, such as optics and coherent photonics, to improve early diagnostic and therapeutic procedures to reduce cancer incidence and mortality.

The development of optical methods in modern medicine in the field of diagnostics, surgery, and therapy has stimulated the study of the optical properties of human and animal tissues, since the efficiency of optical sensing of tissues depends on the photon propagation and fluence rate distribution [2].

Examples of diagnostic use are the following: monitoring of blood oxygenation and tissue metabolism, analysis of main tissue components, detection of malignant neoplasms, and recently proposed various techniques for optical imaging. The latter is particularly interesting for virtual optical biopsy and the precise determination of tumor boundaries during surgical operations. Therapeutic usage mostly includes applications in photodynamic therapy. For all these applications, knowledge of the optical properties of tissues is of great importance for the interpretation and quantification of diagnostic data and for predicting the distribution of light and absorbed energy for therapeutic and surgical use.

In this chapter, we provide an overview of the optical properties of benign and malignant tumors measured over a wide wavelength range and discuss the main cancer markers for various types of tumors.

1.2 Tumor Optical Properties Measurements: A Brief Description

Among the numerous methods for measuring the optical properties of tissue, the most widely used are integrating spheres spectroscopy, reflectance spectroscopy as well as Raman and fluorescence spectroscopy.

Iterative methods for processing experimental data, as a rule, take into account discrepancies between the refractive indices at the boundaries of the sample as well as the multilayer nature of the sample. The following factors are responsible for the errors in the estimated values of the optical coefficients and need to be borne in mind in a comparative analysis of the optical parameters obtained in various experiments [3]:

- The physiological conditions of tissues (the degree of hydration, homogeneity, species-specific variability, frozen/thawed or fixed/unfixed state, *in vitro*/*in vivo* measurements, smooth/rough surface);
- The geometry of irradiation;
- The matching/mismatching interface refractive indices;
- The numerical aperture of photodetectors;
- The separation of radiation experiencing forward scattering from unscattered radiation;
- The theory used to solve the inverse problem.

To analyze the propagation of light under multiple scattering conditions, it is assumed that absorbing, fluorescence, and scattering centers are uniformly distributed across the tissue. UV-A, visible, or NIR radiation is usually subjected to anisotropic scattering characterized by a clearly apparent direction of photons undergoing single scattering, which may be due to the presence of large cellular organelles (mitochondria, lysosomes, Golgi apparatus, etc.) [3–5].

When the scattering medium is illuminated by unpolarized light and/or only the intensity of multiply scattered light needs to be computed, a sufficiently strict mathematical description of continuous wave (CW) light propagation in a medium is possible in the framework of the scalar stationary radiation transfer theory (RTT) [3–6]. This theory is valid for an ensemble of scatterers located far from each other and has been successfully used to develop some practical aspects of tissue optics. The main stationary equation of RTT for average spectral power flux density $I_\lambda\left(\vec{r},\vec{s}\right)$ (in W/cm^2 sr) for wavelength λ at point $\vec{r}$ in the given direction $\vec{s}$ and monochromatic irradiation has the form

$$\frac{\partial I_\lambda\left(\vec{r},\vec{s}\right)}{\partial s} = -\mu_t I_\lambda\left(\vec{r},\vec{s}\right) + \frac{\mu_s}{4\pi}\int_{4\pi} I_\lambda\left(\vec{r},\vec{s}\right) p\left(\vec{s},\vec{s}'\right) d\Omega' + \varepsilon\left(\vec{s},\vec{s}'\right), \tag{1.1}$$

where $p\left(\vec{s},\vec{s}'\right)$ is the scattering phase function, 1/sr; $d\Omega'$ is the unit solid angle about the direction $\vec{s}'$, sr; $\mu_t = \mu_a + \mu_s$ is the total attenuation coefficient, 1/cm; μ_a is the absorption coefficient, 1/cm; μ_s is the scattering coefficient, 1/cm; and $\varepsilon\left(\vec{s},\vec{s}'\right)$ is the internal light source, which accumulates the effects of fluorescence and Raman spectroscopy. However, in most practically interesting cases, the measurement of the absorption and scattering coefficients of tissues can be performed neglecting the effects of fluorescence and Raman scattering, since their quantum efficiency is relatively small. It is equivalent to Eq. (1.1) in the absence of the internal radiation sources.

The scalar approximation of the radiative transfer equation (RTE) gives poor accuracy when the size of the scattering particles is much smaller than the wavelength, but provides acceptable results for particles comparable to and exceeding the wavelength [7].

The phase function $p\left(\vec{s},\vec{s}'\right)$ describes the scattering properties of the medium and is actually the probability density function for scattering in the direction $\vec{s}'$ of a photon traveling in the direction $\vec{s}$; in other words, it characterizes an elementary scattering event. If scattering is symmetric relative to the direction of the incident wave, then the phase function depends only on the scattering angle θ (angle between directions $\vec{s}$ and $\vec{s}'$), i.e., $p\left(\vec{s},\vec{s}'\right) = p\left(\theta\right)$. The assumption of random distribution of scatterers in a medium (i.e., the absence of spatial correlation in the tissue structure) leads to normalization:

$$\int_0^\pi p\left(\theta\right) 2\pi \sin\theta d\theta = 1.$$

In practice, the phase function is usually well approximated with the aid of the postulated Henyey–Greenstein function [2–6, 8]:

$$p(\theta) = \frac{1}{4\pi} \frac{1 - g^2}{\left(1 + g^2 - 2g\cos\theta\right)^{3/2}}, \tag{1.2}$$

where g is the scattering anisotropy parameter (mean cosine of the scattering angle θ):

$$g = <\cos\theta> = \int_0^{\pi} p(\theta)\cos\theta 2\pi \sin\theta d\theta.$$

The value of g varies in the range from -1 to 1; $g = 0$ corresponds to isotropic (Rayleigh) scattering, $g = 1$ to total forward scattering (Mie scattering at large particles), and $g = -1$ to total backward scattering [3–9].

Other phase functions commonly used to analyze the propagation of light in turbid media, including tissue, are the small-angle scattering phase function [10, 11], the Mie phase function [12–15], the δ-Eddington phase function [16, 17], the Reynolds–McCormick phase function [18–20], the Gegenbauer kernel phase function [14, 15, 21, 22], and their modifications [23–25].

1.2.1 Integrating Sphere Spectroscopy

Integrating sphere spectroscopy (ISS) is commonly used as an optical calibration and measurement tool and, in particular, it is successfully used to measure optical properties of tissues [2, 3, 5]. A detailed theory of the integrating sphere spectroscopy is presented in [26–32]. The inner surface of an integrating sphere is uniformly coated with highly reflective diffuse materials (exceeding 0.98) to achieve homogenous distributions of light radiation at the sphere's inner wall. A light beam falling on the inner surface of an integrating sphere is evenly scattered to all directions (Lambertian reflections) and the light fluxes are evenly distributed (spatially integrated) on the homogenous inner surface of the sphere after multiple Lambertian reflections. A standard integrating sphere usually has three ports: an input port, an output port, and a third port for the detector. In certain applications, the fourth port is also used so that the specular reflection beam can go out from the sphere in a light trap. However, for real integrating spheres, the surfaces do not have perfect Lambertian reflection. To prevent measurement errors by specular reflection, baffle(s) coated with a highly reflective material is often placed inside the sphere to further diffuse the specular reflection and avoid the direct reflection from reaching the detector.

There are several advantages of using spectroscopy with integrating sphere for measuring the spectral reflectance and transmittance of tissue samples, in

comparison with direct measurement of the samples by a spectrometer. First, in a regular spectrometer measurement the incident light directly illuminates the sample surface, and the detected reflectance often has a dependency on the angle and distance between the incident beam and the detector. When an integrating sphere is used, all backreflected fluxes are captured and normalized by the sphere. Therefore, the angular dependency is no longer an issue. Second, the detector-object distance is often fixed in the integrating sphere measurement. Even if there is a small change in the sample-sphere distance, it will not affect the results of the measurements as long as all reflected light bounces back into the sphere. Additionally, by using integrating spheres, the spectral measurements are less dependent on the shape of the light beam and the homogeneity of the sample, since both incident light beam and the reflected/scattered light will be normalized on the inner surface of the sphere before being captured by the detector.

The optical parameters of tissue samples (namely the absorption coefficient μ_a, the scattering coefficient μ_s, and the anisotropy factor of scattering g) could be measured by various methods. The single- or double-integrating sphere method combined with collimated transmittance measurement (see Fig. 1.1) is the most often used for *in vitro* tissue studies. Briefly, this approach implies either sequential or simultaneous determination of three parameters: the total transmittance $T_t = T_c + T_d$ (T_d is the diffuse transmittance), the diffuse reflectance R_d, and the collimated transmittance $T_c = I_d/I_0$ (I_d is the intensity of transmitted light measured using a distant photodetector with a small aperture, and I_0 is the intensity of incident radiation).

Any three measurements from the following five are sufficient for the evaluation of all three optical parameters [3]:

1. Total (or diffuse) transmittance for collimated or diffuse radiation;
2. Total (or diffuse) reflectance for collimated or diffuse radiation;
3. Absorption by a sample placed inside an integrating sphere;
4. Collimated transmittance;
5. Angular distribution of radiation scattered by the sample.

The optical parameters of the tissue are deduced from these measurements using different theoretical expressions or numerical simulations: the inverse Monte Carlo (IMC) [33–41] or inverse adding-doubling (IAD) [42–51] methods, or methods based on the diffusion approximation of the transfer equation [52–56]. However, the diffusion approximation has limitations, including describing tissue with a low albedo and accurate consideration of boundary conditions. To overcome these shortcomings other techniques such as the IAD and the IMC are the most commonly used.

The adding-doubling technique is a numerical method for solving the 1D transport equation in slab geometry. It can be used for tissue with an arbitrary phase function, arbitrary angular distribution of the spatially uniform incident radiation, and infinite beam size as lateral light losses cannot be taken into account. The angular distribution of the reflected radiance (normalized to an incident diffuse flux) is given by Prahl et al. [42]:

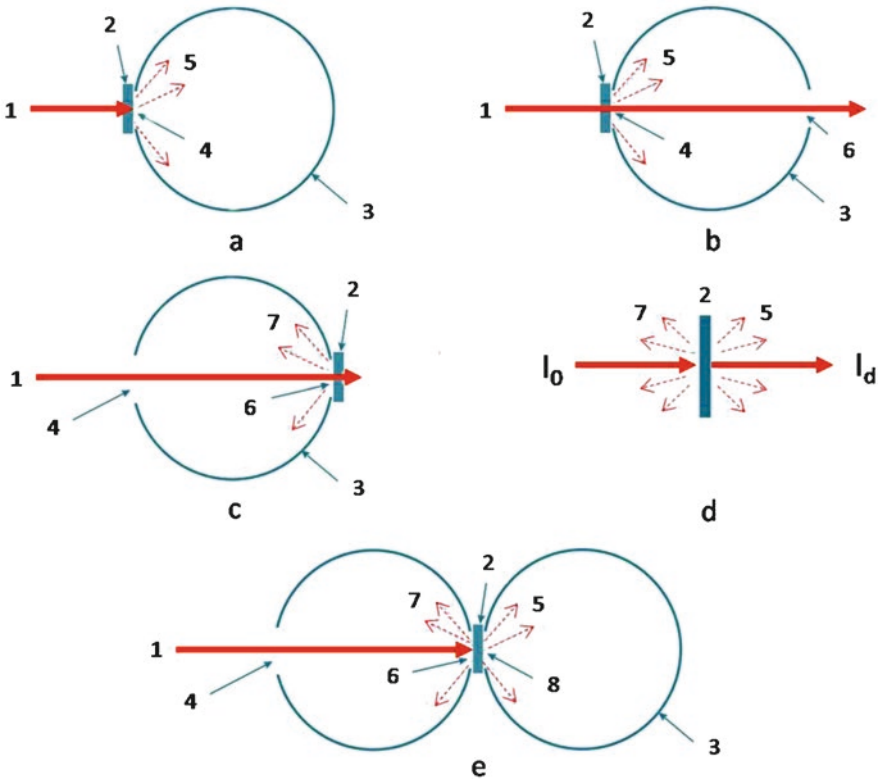

Fig. 1.1 Measurement of tissue optical properties using an integrating sphere. (**a**) Total transmittance mode, (**b**) diffuse transmittance mode, (**c**) diffuse reflectance mode, (**d**) collimated transmittance mode, (**e**) double-integrating sphere. 1 is the incident beam; 2 is the tissue sample; 3 is the integrating sphere; 4 is the entrance port; 5 is the transmitted radiation; 6 is the exit port; 7 is the diffuse reflected radiation

$$I_{\text{ref}}\left(\eta_c\right)=\int_0^1 I_{\text{in}}\left(\eta_c^{'}\right)R\left(\eta_c^{'},\eta_c\right)2\eta_c^{'}d\eta_c^{'}, \tag{1.3}$$

where $I_{\text{in}}(\eta_c)$ is an arbitrary incident radiance angular distribution, η_c is the cosine of the polar angle, and $R\left(\eta_c^{'},\eta_c\right)$ is the reflection redistribution function determined by the optical properties of the slab.

The distribution of the transmitted radiance can be expressed in a similar manner, with obvious substitution of the transmission redistribution function $T\left(\eta_c^{'},\eta_c\right)$. If M quadrature points are selected to span over the interval (0, 1), the respective matrices can approximate the reflection and transmission redistribution functions:

$$R\left(\eta_{\text{ci}}^{'},\eta_{\text{cj}}\right)\rightarrow R_{\text{ij}};\; T\left(\eta_{\text{ci}}^{'},\eta_{\text{cj}}\right)\rightarrow T_{\text{ij}}. \tag{1.4}$$

These matrices are referred to as the reflection and transmission operators, respectively. If a slab with boundaries indexed as 0 and 2 is comprised of two layers, (01) and (12), with an internal interface 1 between the layers, the reflection and transmission operators for the whole slab (02) can be expressed as:

$$\boldsymbol{T}^{02} = \boldsymbol{T}^{12}\left(\boldsymbol{E} - \boldsymbol{R}^{10}\boldsymbol{R}^{12}\right)^{-1}\boldsymbol{T}^{01},$$

$$\boldsymbol{R}^{20} = \boldsymbol{T}^{12}\left(\boldsymbol{E} - \boldsymbol{R}^{10}\boldsymbol{R}^{12}\right)^{-1}\boldsymbol{R}^{01}\boldsymbol{T}^{12} + \boldsymbol{R}^{21},$$

$$\boldsymbol{T}^{20} = \boldsymbol{T}^{10}\left(\boldsymbol{E} - \boldsymbol{R}^{12}\boldsymbol{R}^{10}\right)^{-1}\boldsymbol{T}^{21},$$

$$\boldsymbol{R}^{02} = \boldsymbol{T}^{10}\left(\boldsymbol{E} - \boldsymbol{R}^{12}\boldsymbol{R}^{10}\right)^{-1}\boldsymbol{R}^{12}\boldsymbol{T}^{01} + \boldsymbol{R}^{10}, \tag{1.5}$$

where $\boldsymbol{E}$ is the identity matrix defined in this case as:

$$E_{\mathrm{ij}} = \frac{1}{2\eta_{\mathrm{ci}} w_i}\delta_{\mathrm{ij}}, \tag{1.6}$$

where w_i is the weight assigned to the i-th quadrature point and δ_{ij} is a Kronecker delta symbol, $\delta_{\mathrm{ij}} = 1$ if $i = j$, and $\delta_{\mathrm{ij}} = 0$ if $i \neq j$.

The definition of the matrix multiplication also slightly differs from the standard. Specifically,

$$\left(\boldsymbol{AB}\right)_{\mathrm{jk}} \equiv \sum_{j=1}^{M} A_{\mathrm{ij}} 2\eta_{\mathrm{cj}} w_j B_{\mathrm{jk}}. \tag{1.7}$$

Equations (1.5) allow one to calculate the reflection and transmission operators of a slab when those of the comprising layers are known. The idea of the method is to start with a thin layer for which the RTE can be rather easily simplified and solved, producing the reflection and transmission operators, and then proceed by doubling the thickness of the layer until the thickness of the whole slab is reached. Several techniques exist for layer initialization. The single-scattering equations for reflection and transmission for the Henyey–Greenstein function are given by van de Hulst [57] and Prahl [58]. The refractive index mismatch can be taken into account by adding effective boundary layers of zero thickness and having the reflection and transmission operators determined by Fresnel's formulas. Both total transmittance and reflectance of the slab are obtained by straightforward integration of Eq. (1.3). Different methods of performing the integration and the IAD program provided by S. A. Prahl [42, 58] allow one to obtain the absorption and the scattering coefficients from the measured diffuse reflectance R_{d} and total transmittance T_t of the tissue slab. This program is the numerical solution to the steady-state RTE (Eq. (1.1)) realizing an iterative process, which estimates the reflectance and transmittance from a set of optical parameters until the calculated reflectance and transmittance match the

measured values. Values for the anisotropy factor g and the refractive index n must be provided to the program as input parameters.

It was shown that using only four quadrature points, the IAD method provides optical parameters that are accurate to within 2–3% [42]. Higher accuracy, however, can be obtained by using more quadrature points, but it would require increased computation time. Another valuable feature of the IAD method is its validity for the study of samples with comparable absorption and scattering coefficients [42], since other methods based on only diffusion approximation are inadequate. Furthermore, since both anisotropic phase function and Fresnel reflection at boundaries are accurately approximated, the IAD technique is well suited to optical measurements of biological tissues and blood held between two glass slides. The adding-doubling method provides accurate results in cases when the side losses are not significant, but it is less flexible than the Monte Carlo (MC) technique.

Both the real geometry of the experiment and the tissue structure may be complicated. Therefore, inverse Monte Carlo method has to be used if reliable estimates are to be obtained. A number of algorithms to use the IMC method are available now in the literature [5, 15, 19, 33, 37–39, 59–61]. Many researches use the Monte Carlo (MC) simulation algorithm and program provided by S. L. Jacques, and L. Wang et al. [35, 62, 63]. The MC technique is employed as a method to solve the forward problem in the inverse algorithm for the determination of the optical properties of tissues and blood. The MC method is based on the formalism of the RTT, where the absorption coefficient is defined as a probability of a photon to be absorbed per unit length, and the scattering coefficient is defined as the probability of a photon to be scattered per unit length. The effects of fluorescence and Raman scattering may be also taken into account in a similar way by introducing the probability of generating new photons with different frequencies for the correspondingly absorbed or scattered initial photons. Using these probabilities, a random sampling of photon trajectories is generated. Among the firstly designed IMC algorithms, similar algorithms for determining all three optical parameters of the tissue (μ_a, μ_s, and g) based on the *in vitro* evaluation of the total transmittance, diffuse reflectance, and collimated transmittance using a spectrophotometer with integrating spheres can be also mentioned [5, 15, 33, 37, 38, 40, 41, 44, 50, 60, 61, 64]. The initial approximation (to speed up the procedure) is achieved with the help of the Kubelka–Munk theory, specifically its four-flux variant [3, 5, 33, 37, 38, 65–67]. The algorithms take into consideration the sideways loss of photons, which becomes essential in sufficiently thick samples. Similar results have been obtained using the condensed IMC method [5, 60, 61, 68–73]. Figure 1.2 demonstrates the typical flowchart of the IMC method [41].

In the basic MC algorithm a photon described by three spatial coordinates and two angles (x, y, z, θ, ϕ) is assigned its weight $W = W_0$ and placed in its initial position, depending on the source characteristics. The step size s of the photon is determined as $s = -\ln(\xi)/\mu_t$, where ξ is the random number between (0, 1). The direction of the photon's next movement is determined by the scattering phase function substituted as the probability density distribution. Several approximations for the scattering phase function of tissue and blood have been used in MC simulations. They

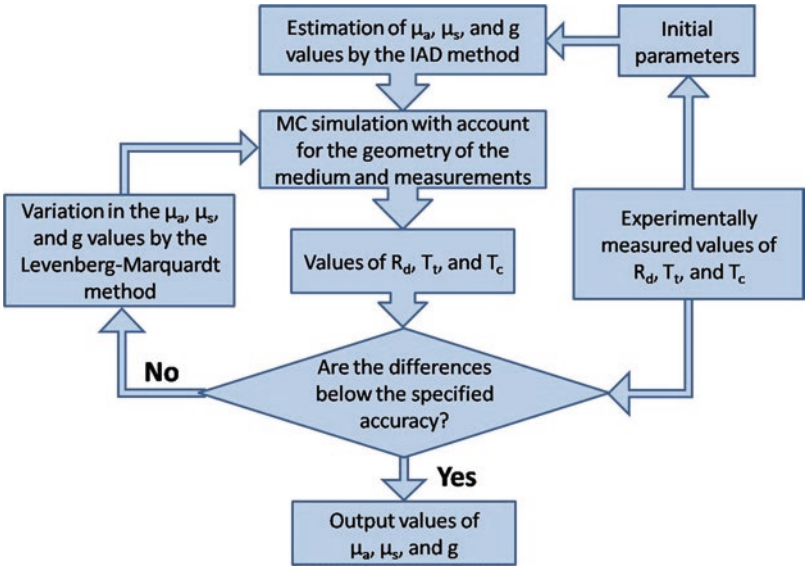

Fig. 1.2 The typical flowchart of the IMC method [41]

include two empirical phase functions widely used to approximate the scattering phase function of tissue and blood, Henyey–Greenstein phase function (HGPF) (see Eq. (1.2)), the Gegenbauer kernel phase function (GKPF), and Mie phase function.

In most cases, azimuthal symmetry is assumed. This leads to $p(\phi) = 1/2\pi$ and, consequently, $\phi_{\text{rnd}} = 2\pi\xi$. At each step, the photon loses part of its weight due to absorption: $W = W(1 - \Lambda)$, where $\Lambda = \mu_s/\mu_t$ is the albedo of the medium.

When the photon reaches the boundary, part of its weight is transmitted according to the Fresnel equations. The amount transmitted through the boundary is added to the reflectance or transmittance. Since the refraction angle is determined by the Snell's law, the angular distribution of the out-going light can be calculated. The photon with the remaining part of the weight is specularly reflected and continues its random walk.

When the photon's weight becomes lower than a predetermined minimal value, the photon can be terminated using "Russian roulette" procedure [35, 62, 63]. This procedure saves time, since it does not make sense to continue the random walk of the photon, which will not essentially contribute to the measured signal. On the other hand, it ensures that the energy balance is maintained throughout the simulation process.

The MC method has several advantages over the other methods because it may take into account mismatched medium-glass and glass-air interfaces, losses of light at the edges of the sample, any phase function of the medium, and the finite size and arbitrary angular distribution of the incident beam. The only disadvantage of this method is the long time needed to ensure good statistical convergence, since it is a statistical approach. The standard deviation of a quantity (diffuse reflectance,

transmittance, etc.) approximated by MC technique decreases proportionally to $1/\sqrt{N}$, where N is the total number of launched photons. It is worthy of note that stable operation of the algorithm is maintained by generation of from 10^5 to 5×10^5 photons per iteration. Two to five iterations are usually necessary to estimate the optical parameters with approximately 2% accuracy.

1.2.2 Diffuse Backscattered Reflectance Spectroscopy

Diffuse backscattered reflectance spectroscopy (BS) [5, 72–87] is well suited for use in biomedical applications due to its low instrumentation cost, easy implementation, and non-destructive measurement setup. Hence, many different BS measurement configurations have been developed. Optical fiber arrays and non-contact reflectance imagery are two typical sensing configurations in BS measurement, which can be implemented with fiber-optic probe (FOP), monochromatic imaging (MCI), and hyperspectral imaging (HSI). In the FOP measurement, a single spectrometer, multiple spectrometers, or a spectrograph-camera combination coupled with multiple detection fibers can be used to measure diffuse reflectance at different distances from the light incident point. Moreover, it is also desirable to measure a tissue sample at a greater depth. To overcome the shortcomings of a rigid FOP, a flexible FOP with numerous optical fibers covering a spatial distance range of 0–30 mm can be used for measuring the tissue optical properties. Optical fibers have to be coupled to a multichannel hyperspectral imaging system, which allows simultaneous acquisition of reflectance spectra from the sample. The use of several different sizes of fibers for the probe also expands effectively the dynamic range of the camera, allowing acquiring spectra at greater depth of the sample.

As a non-contact method, MCI is more suitable for measuring optical properties of tissues for monochromatic irradiation. A laser diode or a combination of a supercontinuum laser and a monochromator can be used to illuminate a sample at a specific wavelength. The diffuse reflectance is acquired with a CCD camera. This BS configuration is simple and relatively easy to implement. The acquired 2D scattering images are reduced to 1D scattering profiles by radial averaging when the scattering images are axisymmetric with respect to the laser incident point. However, this assumption is not satisfied for anisotropic tissues where the light is guided by the tissue fibers. For example, in the case of bovine muscle tissue, the effect of the fibers resulted in scatter spots with a rhombus shape. Measurement at multiple wavelengths requires sequential wavelength scanning. In addition, a substantial portion of the signal of each pixel comes from the surrounding areas, which may affect the accuracy of the measurement. Therefore, the characterization of the point-spread function (PSF) is necessary in order to minimize errors in the obtained intensity values for the image data interpretation.

In the hyperspectral imaging, spectral and spatial information is acquired simultaneously and, therefore, it has advantageous for measuring diffuse reflectance profiles over a broad spectral range. As a rule typical hyperspectral imaging-based BS

system in line scan mode has high spatial resolution and mainly consists of a high-performance CCD camera, an imaging spectrograph, a zoom or prime lens, a light source, and an optical fiber coupled with a focusing lens for delivering a broadband beam to the sample.

As an indirect method for optical property measurement, computation of the optical parameters from the BS measurements usually requires sophisticated modeling based on the diffusion approximation of radiative transfer theory or MC simulation, coupled with appropriate inverse algorithms. Numerical methods are generally required for solving the radiative transfer equation or using inverse MC simulation. These methods are flexible and allow possibility for modeling of different geometries of experimental setups but they may be subjected to statistical uncertainties during the estimation of the reflectance. Moreover, one of the major drawbacks with the numerical methods is that they require substantial computational time. To overcome the shortcomings the condensed IMC method can be used, that is, a library of MC simulated BS profiles for a grid of μ_s, μ_a and g values can be calculated, and then the library can be used either as a look-up table or for training a neural network.

Another way to reconstruct the tissue optical parameters (such as μ_a and reduced scattering coefficient $\mu_s' = \mu_s(1-g)$) has been proposed by Zonios et al. [88–91]. Their approach is based on diffusion approximation and assumes that $R(\lambda) = \dfrac{\mu_s'(\lambda)}{k_1 + k_2 \mu_a(\lambda)}$. Here $R(\lambda)$ is the diffuse reflectance, λ is the wavelength, k_1 and k_2 are constants that depend on the probe geometry. The optical coefficients μ_a and μ_s' can be related to the absorption and scattering properties of the tissue through Eqs. (1.8) and (1.9) (for example):

$$\begin{aligned}\mu_a(\lambda) = C_{\mathrm{Hb}}\left[\alpha \cdot \varepsilon_{\mathrm{HbO}}(\lambda) + (1-\alpha)\varepsilon_{\mathrm{Hb}}(\lambda)\right] + C_w \cdot \varepsilon_w(\lambda) \\ + C_{\mathrm{mel}} \cdot \varepsilon_{\mathrm{mel}}(\lambda) + C_{\mathrm{col}} \cdot \varepsilon_{\mathrm{col}}(\lambda) + \ldots,\end{aligned} \tag{1.8}$$

where C_{Hb} is the total concentration of hemoglobin, α is the oxygen saturation of hemoglobin, C_w is the concentration of water, C_{mel} is the concentration of melanin, C_{col} is the concentration of collagen, and $\varepsilon_{\mathrm{HbO}}$, $\varepsilon_{\mathrm{Hb}}$, ε_w, $\varepsilon_{\mathrm{mel}}$, $\varepsilon_{\mathrm{col}}$ are the absorption coefficients of oxyhemoglobin, deoxyhemoglobin, water, melanin, and collagen, respectively.

$$\mu_s'(\lambda) = \frac{A}{\lambda^w}, \tag{1.9}$$

where parameter A is defined by the concentration of scattering particles in the tissue, and the wavelength exponent w is independent of the particles concentration, characterizes the mean size of the particles, and defines the spectral behavior of the scattering coefficient [92].